ARTICLE　　OPEN

Check for updates

Computational demystification of iron carbonyls formation under syngas environment

El Tayeb Bentria (ID)[1], Prathamesh Mahesh Shenai[2], Stefano Sanvito[3], Heesoo Park (ID)[4], Laurent Karim Béland[5], Nicholas Laycock[6] and Fedwa El Mellouhi (ID)[1 ✉]

Iron pentacarbonyl (IPC) gas forms upon the reaction of carbon monoxide with Fe containing metallic surfaces under gas reforming conditions. IPC formation can sometimes reach alarming levels that cause metal loss, pipeline thinning corrosion, catalyst poisoning, and contamination of sensitive industrial equipment. In this work, we demystify using multiscale computational modeling the mechanism of Iron pentacarbonyl formation: Density functional theory (DFT) is used to explore various catalytic reactions that involve a Fe adatom reacting with adsorbed carbon monoxide. Our calculated carbonyls desorption barriers on a perfect and clean Fe surface are too high to allow the carbonyls to form then desorb at temperatures <500 K at the rates reported experimentally. Most importantly, our calculations indicate that a high CO surface coverage, in addition to the presence of Fe adatoms, favors carbonyl formation and its desorption towards the flowing gas medium. Using insights extracted from ab initio molecular dynamics simulations, we propose that the most plausible IPC formation mechanism consists of: (1) on surface reactions of adsorbed CO molecules with an Fe adatom to form iron tricarbonyl ($Fe(CO)_3^*$) molecules; (2) an adsorbate assisted movement of iron tricarbonyl on top of the CO adlayer; and (3) the interaction of iron tricarbonyl with CO molecules from the gaseous medium eventually leading to iron adatom removal as $Fe(CO)_5$ gas.
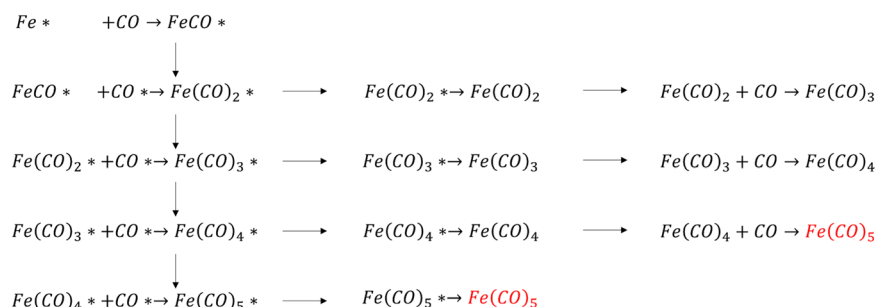
INTRODUCTION

Gaseous carbon monoxide is considered relatively inert when interacting with metals at ambient temperature and atmospheric pressure. However, at higher pressures it exhibits a complex set of interactions with metallic surfaces via chemisorption and bond dissociation that led to a number of different effects and implications[1]. It is known that CO can form metal carbonyl complexes that can be volatile and hence remove the metal atoms from the surface, causing surface degradation and corrosion[2]. Iron pentacarbonyl (IPC), or $Fe(CO)_5$, is a highly toxic and flammable compound that can form on surfaces of ferrous alloys (usually steel) over ~400 K to 573 K and at moderate to high pressures[2]. CO and synthetic gas (mixture of CO and H_2) are important industrial gases and the formation of IPC in industrial systems containing CO environment can lead to problems not just related to corrosion, but also with respect to toxicity and other detrimental effects in downstream process units. IPC is known, for example, to deactivate and poison catalysts and contaminate semiconductor fabrication and lab equipments[1,3]. Carbonyl corrosion is a form of surface attack that causes wall thinning rather than structural changes deep inside the steel, such as intergranular or corrosion cracking[2].

IPC was first observed in 1891 as a reaction product of syngas and carbon steel[4], and identified in 1958 by Cotton et al.[5]. Multiple following studies attempted to quantify the IPC formation rate as function of the reactor operating conditions and syngas composition as well as to understand the IPC formation mechanism[2,6–8]. Inouye et al.[6] used an atomic absorption spectrophotometer to measure the rate of formation of iron carbonyl in 1–2% Mo steel pipes as a function of gas velocity, temperature, pressure, and gas composition. The rate of formation of iron carbonyl was found to increase linearly with the gas velocity until it reaches saturation. This occurs above a critical velocity when equilibrium is not maintained. They found that carbonyl corrosion could also occur upon exposure to pure CO gas, reaching its maximum when the temperature reaches 518 K. This is higher than the 450 K maximum obtained when syngas is used instead. Experiments also show iron carbonyl formation to become negligible once the temperature is increased beyond 550 K[2,6]. Later, J. Brynestad et al.[9] accounted for other parameters such as impurities in the gas, metallic alloy composition, surface conditions, and pretreatment of the surfaces. In particular, gaseous $Fe(CO)_5$ dissociation has attracted the interest of the scientific community in recent years. For example, work was conducted by ultrafast mid-infrared transient absorption spectroscopy and density functional theory (DFT) calculations to study the sequential dissociation of iron pentacarbonyl to form iron tricarbonyl $Fe(CO)_3$ via a short lived iron tetracarbonyl $Fe(CO)_4$ intermediate[10]. Furthermore, a few DFT calculations have been carried out on Fe(CO)5 (and other metal carbonyls). Most of the previous works focused on the IPC structure[11–13], particularly with the difference between the axial and equatorial Fe−C and C−O bond lengths as well as the dissociation energy of the ligand decoordination reaction, $Fe(CO)_5 \rightarrow Fe(CO)_4 + CO$, and the vibrational interchange between the axial and equatorial CO groups via the Berry pseudo-rotation mechanism[12].

A significant number of computational studies have dealt with CO chemisorption on Fe surfaces. Nevertheless, little effort has been made to address, at the atomistic scale, how the carbonyl species are actually formed upon CO adsorption on the metallic

[1]Qatar Environment and Energy Research Institute, Hamad Bin Khalifa University, P.O. BOX 34110, Doha, Qatar. [2]Shell Technology Centre Bangalore, Bengaluru 562149, India. [3]School of Physics, AMBER and CRANN Institute, Trinity College, Dublin 2, Ireland. [4]Centre for Material Science and Nanotechnology, Department of Chemistry, University of Oslo, Oslo, Norway. [5]Department of Mechanical and Materials Engineering, Queen's University, Kingston, ON K7L3N6, Canada. [6]Qatar Shell Research and Technology Centre, Qatar Science and Technology Park, Doha 24750, Qatar. ✉email: felmellouhi@hbku.edu.qa

$$Fe* \qquad +CO \rightarrow FeCO*$$

$$FeCO* \quad +CO* \rightarrow Fe(CO)_2* \quad \longrightarrow \quad Fe(CO)_2* \rightarrow Fe(CO)_2 \quad \longrightarrow \quad Fe(CO)_2 + CO \rightarrow Fe(CO)_3$$

$$Fe(CO)_2* + CO* \rightarrow Fe(CO)_3* \quad \longrightarrow \quad Fe(CO)_3* \rightarrow Fe(CO)_3 \quad \longrightarrow \quad Fe(CO)_3 + CO \rightarrow Fe(CO)_4$$

$$Fe(CO)_3* + CO* \rightarrow Fe(CO)_4* \quad \longrightarrow \quad Fe(CO)_4* \rightarrow Fe(CO)_4 \quad \longrightarrow \quad Fe(CO)_4 + CO \rightarrow Fe(CO)_5$$

$$Fe(CO)_4* + CO* \rightarrow Fe(CO)_5* \quad \longrightarrow \quad Fe(CO)_5* \rightarrow Fe(CO)_5$$

Fig. 1 Schematic representation of pathways considered in this study leading to iron pentacarbonyl formation on Fe surface exposed to CO gas. The species marked with * represent surface adsorbed species and those without the * represent gas phase molecules.

surface. Among these efforts, Cheng et al.[13], >20 years ago, employed DFT calculations to investigate the desorption of IPC from Fe(110) surface and found a desorption barrier of 3.88 eV. To the best of our knowledge, no similar atomistic investigations followed. In this article, we use a combination of ab initio molecular dynamics simulations followed by adsorption energy and barrier calculations to compute the energetics of different pathways leading to carbonyls formation on a pure iron surface. Together with mapping the desorption energies of $Fe(CO)_x$, $x = 1–5$, we investigate the effect of CO surface coverage in reducing the reaction and desorption barriers. Finally, we propose and discuss the most probable reaction path leading to IPC formation in a pure CO environment.

We have considered multiple possible IPC formation pathways. Notably, the scenario where IPC forms directly from ad-molecular species adsorbed on the iron surface (Fe) in the form of $Fe(CO)^*_x$ with $x = 1–5$ via sequential reaction with absorbed CO on the surface, denoted herein as CO*. We have also considered an alternative scenario where a subset of reactions occur on the surface to form $Fe(CO)^*_x$ with $x = 2–4$ that subsequently desorb to react further with gaseous CO (g). Figure 1 summarizes the IPC formation pathways that have been considered: Fe* represents an iron atom on an Fe surface that will react with adsorbed CO molecules forming carbonyl species until forming $Fe(CO)_5$ on the surface (Fig. 7a–d) that then desorbs. Alternatively, sub carbonyl species formed on the surface may also desorb and the subsequent reactions might occur in the gas phase, forming IPC as the final product.

This work is the first step in developing fundamental understanding on the mechanisms that govern formation of iron pentacarbonyls over steel surfaces exposed to syngas environments and the effect of gaseous impurities. It is known in literature that the iron pentacarbonyl formation is affected by impurities/contaminants in the gas stream and in some cases can also get accelerated. However, little to no mechanistic understanding exists in literature to the best of our knowledge, which is the primary gap we are attempting to bridge through this work. Modeling realistic steel surfaces is highly challenging as the surface state may entail a complex composition of oxides or carbide depending upon the gas composition and temperature. In this paper, we take the first step, with a simple model surface for steel in the form of pristine iron surfaces. This allows us to extract insights and features of interaction of CO with iron surfaces eventually leading to the formation of iron pentacarbonyl in a simplified and computationally tractable manner. It also provides a reference case that we can potentially test the effects of gas impurities against in future studies. We intend to further build upon the insights derived in this work and extend the models to more complex and closer to realistic surfaces in future.

RESULTS

In this section, we will compute the energetics for carbonyls formation and desorption on Fe(110) surface, and demonstrate that carbonyls are unstable at low CO coverage. We subsequently account for the effect of CO converge on the carbonyls' stability, formation and desorption. Finally, we will describe a two step desorption path for IPC that represent well the experimental observations.

In this section, we describe the computed energy surface for IPC formation on Fe(110) surface containing one adatom and in the limit of low CO concentration on the surface. The first reaction scheme investigated follows Fig. 1 in which the Fe adatom bonds with one CO molecule adsorbed at an adjacent surface site in each reaction step to progressively form $Fe(CO)_x$ with x = 1 to 4. This is shown in Supplementary Fig. 1. We find that for path 1 each of these reaction steps, has no definitive transition state and the reaction barriers are the same as the reaction energies. The formation of $Fe(CO)_4$ requires energy barrier of 1.39 eV. We also propose another possible pathway (path 2) in which two CO* molecules simultaneously react with the Fe(CO)* species to form $Fe(CO)_3^*$. Even if the final product has the same energy as path 1, this path leads to a slightly reduced total overall energy barrier of 1.19 eV for $Fe(CO)_4^*$ formation (Supplementary Fig. 1). However, regardless of the pathway, we could not successfully construct the subsequent and final step to form $Fe(CO)_5$ purely in a surface reaction, namely with the fifth CO molecule adsorbed on the surface bonding with $Fe(CO)_4^*$ to form $Fe(CO)_5^*$ due to insurmountable steric hindrance. The formation of $Fe(CO)_5^*$ is still possible with an alternate mechanism in which a CO molecule from gas phase adsorbs atop $Fe(CO)_4^*$. In this case we have a barrierless adsorption of 1.9 eV.

Figure 2 shows the adsorption energies of Fe adatom and the carbonyl species ($-E_{Fe(CO)_x}^{ad}$) from the clean Fe(110) surface for different CO coverage. In the absence of any additional preabsorbed CO molecules other than those constituting a given carbonyl specie, as shown by the red symbols in Fig. 2, the $Fe(CO)^*_{x=0-5}$ molecular species' desorption requires energies in the range of 3.5 eV to 4.2 eV. Such high desorption energies along with high endothermicity of the reactions described earlier, renders IPC formation implausible at the moderate temperatures of up to 500 K at which carbonyl corrosion has been typically reported to occur. We note that the low coverage CO case studied in this section is intrinsically more amenable to DFT studies and, due to its simplicity, it represents a good model to derive fundamental insights into reaction mechanisms. However, it does not represent the true surface conditions at high partial pressures of CO and high temperatures. In the next section, we refine the model to include the coverage effects.

Surface coverage depends on pressure and temperature and can be described by the Langmuir isotherm equation. Yu et al.[14] calculated the phase diagram of different coverage CO adsorption on Fe$_2$C(001) surface at different temperatures and CO partial

pressures. Their calculated phase diagram shows stability across a wide region of partial pressure. For example, within the carbonyl formation regime at temperatures ranging in 300–500 K and pressure in 10-300 atm, there is no change in the optimal CO
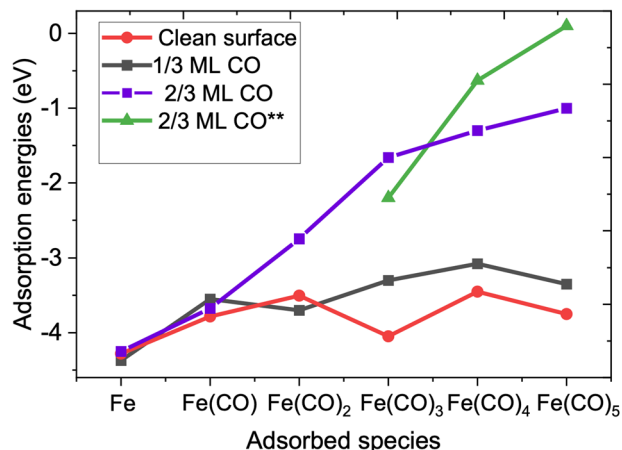

Fig. 2 Adsorption energies of Feadatom and different carbonyl molecular species; on a clean Fe(110) surface (in red), on Fe(110) surface with 1/3 ML CO coverage (in black), and on Fe(110) surface with 2/3 ML CO coverage (in purple). The green curve represents carbonyl species adsorbed on top of CO adlayer rather than the Fe surface. (ML monolayer).

coverage. Temperatures up to 900 K led to a 20% to 30% increase in surface coverage only. Wang el al.[15] used DFT to study the co-adsorption of CO and H_2, and found out that, while CO block H_2 from adsorption, hydrogen pre-coverage hardly affects CO adsorption leading to strong preference of CO pre-coverage on Fe surfaces. These findings indicate that projecting the DFT estimates of surface coverage stability to operational gas pressure and temperature conditions is a sound assumption.

Then, we evaluated different CO coverages on Fe(110) surface in order to select the optimal CO concentration to start with. Supplementary Fig. 2a shows the evolution of the average adsorption energies and the total binding energies calculated using Eq. (2) for Fe(110) surface as a function of surface CO coverage in monolayers (ML). It should be noted that we ran AIMD calculations for each concentration by slowly heating up the system up to 500 K. Then we performed geometry relaxation of the structure from the region that provides the lowest energy [see Supplementary Fig. 2b–e] for the final configurations. This method provides a smoother trend compared to manual construction of a set of adsorption configurations. One can clearly see from Supplementary Fig. 2a that the incremental energy gained by adding one more CO* molecule is almost constant until 2/3 ML coverage, where the average adsorption energy changes from −1.99 to −1.80 eV only. Further addition of CO is thermodynamically favorable up to 0.80 ML. Still, with a weaker reduction in the average adoption energy (red curve Supplementary Fig. 2a) and it continues until the reaction becomes thermodynamically
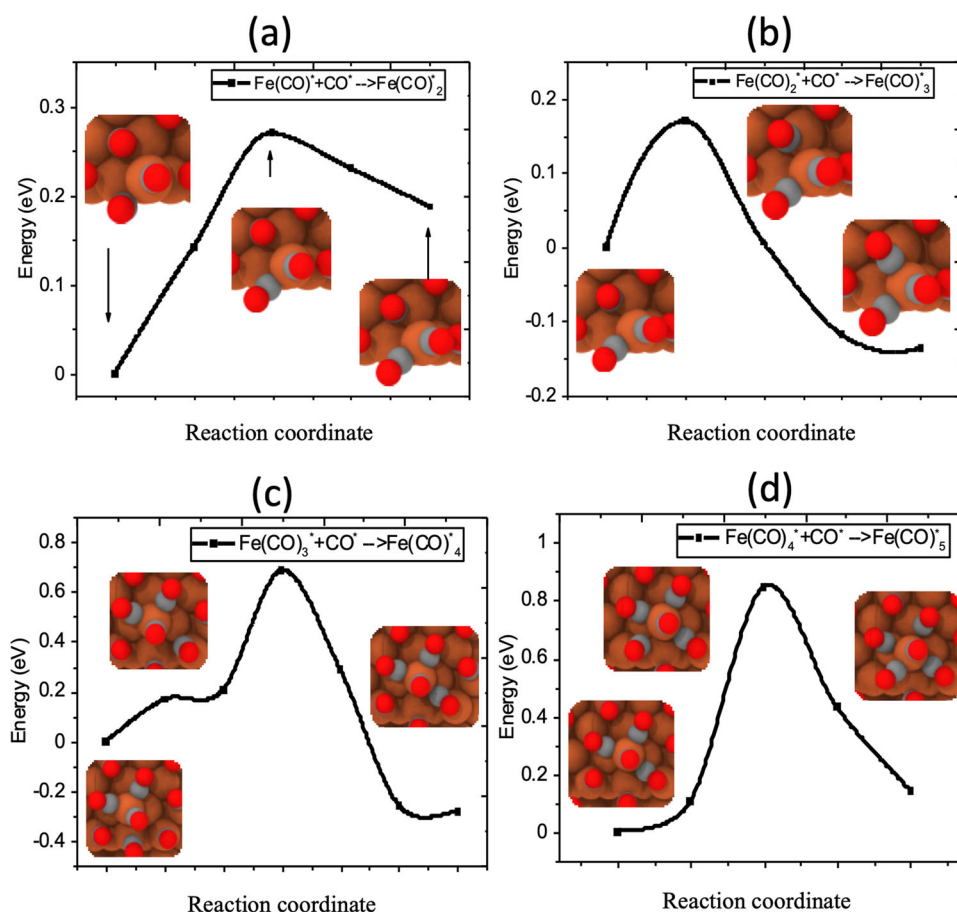
Fig. 3 Reaction pathways and barriers leading to iron-pentacarbonyl formation. Reactions are as follows (**a**) $Fe(CO)^* + CO^* \rightarrow Fe(CO)_2^*$, (**b**) $Fe(CO)_2^* + CO^* \rightarrow Fe(CO)_3^*$, (**c**) $Fe(CO)_3^* + CO^* \rightarrow Fe(CO)_4^*$, (**d**) $Fe(CO)_4^* + CO^* \rightarrow Fe(CO)_5^*$. Fe adatom is bonding with Fe (110) surface in all cases. Color code: oxygen in red, carbon in gray, and iron in brown. The insets on each NEB represents [001] view of the initial and final and saddle point of carbonyl compound.
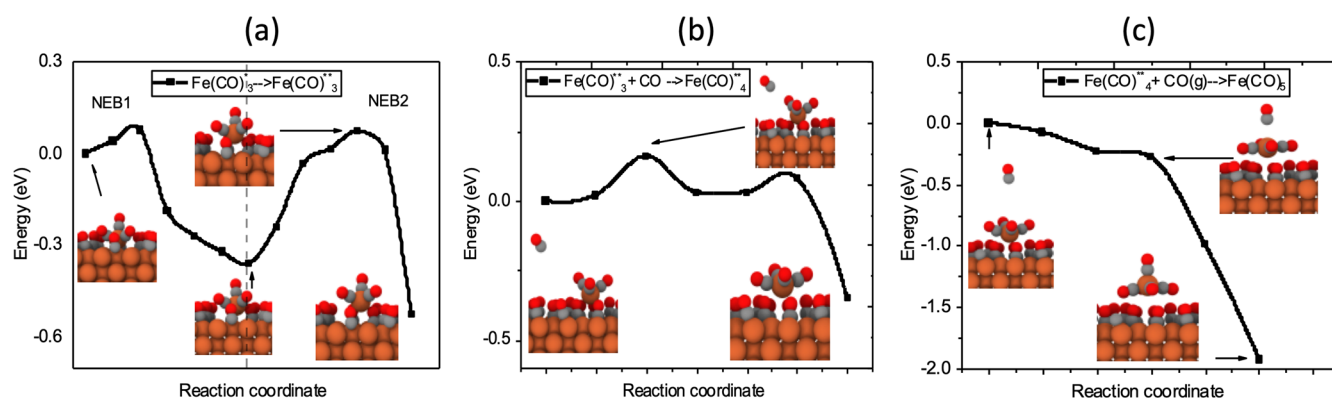
Fig. 4 Reaction path and barriers of Fe(CO)$_3^*$ movement to the adlayer and reacting with CO gas molecules forming IPC. Reaction paths from NEB calculations showing (**a**) the movement of Fe(CO)$_3^*$ to the CO adlayer forming Fe(CO)$_3^{**}$ (video of this reaction is in S.I.), (**b**) the pathway and barrier of Fe(CO)$_3^{**}$ reacting with CO(g) forming Fe(CO)$_4^{**}$, and (**c**) formation of IPC by Fe(CO)$_4^{**}$ binding with CO(g). The insets on each NEB represent [100] view of the initial, final and saddle point of carbonyl compound. Color code: oxygen in red, carbon in gray, and iron in brown.

unfavorable after 0.8 ML, as the convex curve of CO adsorption presented in black confirms.

In our simulation model to evaluate energy surface for IPC formation, we introduce an extra Fe adatom. To partially account for the effect of blocking one higher coordinated metal atom site and introducing a lower coordinated adatom site, we approximate that 2/3 ML CO coverage represents a coverage reasonably close to the optimal one and hence use this model for energy surface computation.

The effect of surface coverage on the desorption energies of each of the carbonyl species as well as the adatom is presented in Fig. 2, where we plot the adsorption energies of Fe(CO)$_{x=0-5}^*$ molecular species, calculated using Eq. (1) in the supplementary information for different CO surface concentrations. Interestingly, there is only a marginal change in adsorption energies at 1/3 ML CO coverage compared to those on the clean surface, with the exception for Fe(CO)$_3^*$. Desorption of any the carbonyl species at this CO coverage would still require at least 3 eV. Fe(CO)$_3^*$ experiences a decrease of 0.6 eV in its adsorption energy at 1/3 ML CO coverage due to the perturbation caused by two nearby CO* molecules to its initially stable configuration on the surface to a configuration where its CO molecules are no longer bound to the surface.

As the CO coverage is increased further to 2/3 ML, one can notice a much more dramatic weakening of the adsorption energy of most of the carbonyl species, especially the change by about 1.8 eV to 1.05 eV for Fe(CO)$_{x=3-5}^*$. These observations are further confirmed by running AIMD simulations for these carbonyls at each surface coverage, where we observe stability of the carbonyl species against decomposition contrary to the Fe(110) clean case.

Figure 3 shows the NEB paths and barriers required to form Fe(CO)$_5^*$ starting from Fe(CO)* in the presence 2/3 ML CO coverage. We can see that starting from Fe(CO)* a cumulative barrier of 0.43 eV is needed for the structure to form a metastable Fe(CO)$_3^*$ complex on the iron surface. Then, a barrier of 0.67 eV needs to be overcome to form a Fe(CO)$_4$ complex, which is 0.2 eV more stable than Fe(CO)$_3^*$, while molecular Fe(CO)$_5^*$ is less likely to form due to the high 0.8 eV reaction barrier.

Even though there is a significant reduction in IPC's overall barrier and desorption energy with CO coverage increased to 2/3 ML, the absolute overall barrier (1.05 eV) for IPC desorption remains quite high to justify desorption from the thermodynamic point of view[6]. An alternative pathway with possibly lower overall barriers was serendipitously discovered via AIMD calculations of systems containing different carbonyl species. We observed on several occasions in the AIMD trajectory, a tendency for the Fe(CO)$_3$ species to exhibit detachment from the Fe surface and

migration atop the CO adlayer (See video 1 and 2 in the supplementary information). This oxygen assisted carbonyl detachment mechanism is governed by Fe(CO)$_x^*$ interactions with vibrating CO* molecules underneath (See videos in the SI). Guided by these insights, we next explored the energetics of carbonyl desorption once subjected to this detachment mechanism. Figure 4a shows the NEBs generated for this path using the final configurations taken from frames of AIMD simulations subjected to full structural relaxation at 0 K. The first NEB (step1-6) represents the movement of Fe(CO)$_3^*$ to the upper surface assisted by O atoms, a process that leads to more stable iron tricarbonyl configuration state where the tricarbonyl is partially detached from the Fe atoms on the surface and compensating with oxygen atoms. Then, the second NEB (step 6-12) represent the movement of the tricarbonyl to the adlayer, in a position where it could easily interact with the CO molecules in the gas, leading to a relaxed state, 0.32 eV more stable than the initial starting configuration denoted as Fe(CO)3**. Figure 4b shows the Eley-Rideal (ER) type of reaction mechanism in which a gas phase CO molecule approaches Fe(CO)$_3$** and binds with it to form Fe(CO)$_4$**. This reaction Fe(CO)$_3^{**}$ + CO(g)--> Fe(CO)$_4^{**}$ requires a barrier of merely 0.16 eV. The subsequent ER reaction with a gas phase CO molecule produces IPC, i.e. Fe(CO)$_4^{**}$ + CO(g)--> Fe(CO)$_5^{**}$, in a barrierless process. These sub-carbonyl species with $x = 4$ and 5, atop the CO adlayer have dramatically weak adsorption energies as evident from the green symbols in Fig. 2. While one can see that Fe(CO)$_3^{**}$ gets slightly more stabilized, Fe(CO)$_4^{**}$ needs only 0.68 eV to desorb. Moreover, Fe(CO)$_5^{**}$ has actually +0.1 eV desorption energy. This means that it repels/desorbs from the surface once it is formed. Thus, we have identified a route for the formation of IPC on Fe(110) containing an Fe adatom. This is not kinetically hindered and has an overall barrier of just 0.43 eV.

DISCUSSION

When considering Fe(CO)$_5^*$ on a clean Fe(110) surface, the calculated desorption energy is 3.75 eV, in good agreement with the only DFT work found in the literature about carbonyl desorption (3.88 eV)[13]. This finding was reinforced by our subsequent calculations of the energies of dissociated carbonyls on a clean Fe surface after structural relaxation Supplementary Table 1. Dissociated carbonyls exhibit more stable energies than systems with formed carbonyls. Thus, we conclude that carbonyls cannot form on a clean Fe surface in the first place.

By elevating the CO coverage to 1/3 ML, the desorption energies exhibit a minor alteration (as depicted in Fig. 2), in contrast to the 2/3 ML CO surface coverage. This implies that a
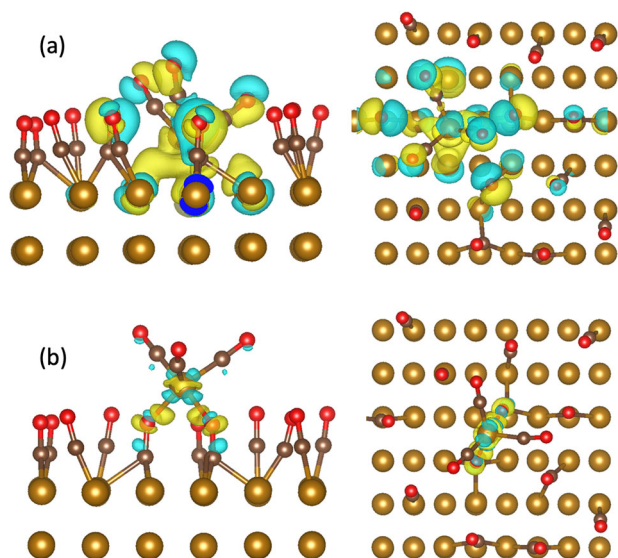
Fig. 5 Electron density difference of Fe(CO)$_3$ on the surface and on top of the CO adlayer. Top and side views of electron density difference isosurface at 0.02 eV of Fe(CO)$_3$ adsorbed on (**a**) Fe(110) surface with 2/3 ML CO coverage, (**b**) on top of CO adlayer. Light blue means charge density depletion, yellow represent charge density accumulation. Color code: oxygen in red, carbon in gray, and iron in brown.

high surface coverage is imperative for carbonyl corrosion, a fact that aligns with experimental findings[6]. The desorption energy of Fe(CO)* is found to be equivalent to that of a clean surface, while a substantial decrease in desorption energy is observed for Fe(CO)$^*_{x=2-3}$, before it gets weaker for Fe(CO)$^*_{x=4-5}$. This behavior can be explained from a geometric perspective. Fe(CO)$^*_{x=1-3}$ have their CO molecules oriented away from the surface, while Fe(CO)$^*_{x=4-5}$ have two of their CO molecules bound to the Fe surface. This makes breaking the Fe-C-Fe and Fe-O-Fe bonds and desorb more challenging. The catalytic reaction of the surface towards C, results in the breaking of C=Fe and C=O double bonds, thus carbon makes a single bond with 3xFe and single bond with O. This specific geometric configuration makes the movement of carbonyl to the adlayer unique to Fe(CO)$_3$ alone. The other paths such as desorption of Fe(CO)$_4^{**}$ is 1.3 eV less stable compared as adsorbate on the Fe slab making its movement to the adlayer unfavorable (see Supplementary Table 2). Fe(CO)$^*_5$, on the other hand, require 0.8 eV barrier to form from Fe(CO)$^*_4$ on the surface. Moreover, Fe(CO)$_2^*$ can go to a 0.3 eV more stable state in the upper layer, but it requires an energy barrier of 0.74 eV to break the strong carbonyl bonding with the Fe surface atoms. The low diffusion barrier of CO molecules on Fe surfaces, coupled with the influence of temperature, leads to oxygen-oxygen repulsion between CO* and Fe(CO)$_3^*$, that with its cone like shape [as depicted in Fig. 5a] favors Fe(CO)$_3^*$ movement to the surface adlayer, with a barrier <0.2 eV. The interesting feature of this 2-step desorption, which has not been documented yet, is that the final state has a reverse barrier of 0.62 eV [Fig. 4a]. Moreover, after the first step desorption, the vibrating CO* molecules on the surface occupy the vacant space created by Fe(CO)$_3^{**}$ preventing it from binding back to the surface.

To express the first desorption step of Fe(CO)$_3^*$, we conducted electron density difference presented in Fig. 5, calculated using Eq. (3) in the (SI). The presence of 0.6 ML of CO molecules on the surface results in decreasing the Fe-C Bond length of Fe(CO)$_3^*$ from 1.84 Å, 1.93 Å and 1.94 Å (compared to tricarbonyl on the same site in a clean Fe surface) to a 1.75 Å, 1.77 Å, and 1.79 Å. This could be explained by the repulsive effect induced by the surrounding CO* molecules, leading to the inability of C atom of

the carbonyl to react with surface Fe atoms. This cone-like shape of Fe(CO)$_3^*$ favors desorption, as it requires only to break the Fe$_{adatom}$-Fe$_{surface}$ bond. Figure 5a illustrates the charge density difference of this system with and without tri-carbonyl; we can see the depletion of charge (in blue) of O-O interaction between Fe(CO)$_3^*$ and its first CO neighbors directed toward the carbonyl. This is a O-lone pair effect as carbon did not participate in this repulsion (no charge density difference observed), meaning the CO bond nature did not change. The accumulation of charge around Fe adatom, simply refer to the bonding of the Fe adatom with the surface comparing to the case in vacuum. Figure 5b shows the energy density difference of Fe(CO)$_3^{**}$ adsorbed of the CO adlayer and Fe(CO)$_3$ in the exact location in the vacuum, From the top view, we can see that the presence of the CO molecules has a minor change in the carbonyl bonding length and geometry, indicating that Fe(CO)$_3$ is taking a relaxed geometry. The bonding of the Fe adatom with the two O atoms with its relaxed shape led to 0.6 eV more stable adsorption energy on the adlayer compared to its adsorption on the surface.

After the Fe(CO)$_3^{**}$ gets lifted on top of CO* molecules, the reaction of the carbonyl with the CO gas molecules becomes more favorable since it does not require Fe-CO* bond breaking as in the case of surface bonding. Another aspect that favors the Fe(CO)$_3^{**}$ + CO (g) type of reaction is the carbonyl CO adlayer bonding that breaks easily when a gaseous CO approaches to react [see Fig. 4b, c]. Fe prefers to bond to C rather than with adlayer dangling O, since Oxygen needs to break its strong double bond with carbon to form a single bond with iron, while carbon can form up to 4 bonds. At a given temperature, there exists an equilibrium concentration of various defects such as adatoms and vacancies, among others, on the surface of iron. The defects can also migrate via surface diffusion. In the adatom model, we relied on so far, we implicitly assumed that a process for generation of Fe adatoms will be available, thereby creating sites for IPC formation. The adatom formation energy is thus an implicit part of the overall energy surface for IPC formation. However, its calculation is nontrivial. For an improved quantitative under-standing of this important aspect, the iron adatom generation section in supplementary materials analyzed a number of different Fe surface models and computed the barriers for the formation of an adatom.

The 0.43 eV barrier required to form IPC found herein applies to a perfect Fe(110) surface; we expect that surface defects such as step edges, grain boundaries, and impurities may affect this barrier further[16]. Also, it is known experimentally that the rate of carbonyl formation is a function of several factors: temperature, pressure, gas flow rate, gas composition, impurities in the gas, alloy composition, surface conditions, and pretreatment of the surfaces, which will be explored in the future[16].

The main reactions studied herein are presented in black (Fig. 6), form the most favorable path for IPC formation on Fe(110) surface. This path is in agreement with the experimental observation of Zaera et al.[17]. We found that Fe(CO)$_5^{**}$ desorb readily after its formation, which is why it was not detected as a surface compound compared to Fe(CO)$_3^{**}$ and Fe(CO)$_4^{**}$, and confirm our finding that IPC cannot form completely on the Fe clean surface at industrial conditions.

On the perfect Fe(110) surface case, the transition states labeled TS2 in Fig. 6 may not be the rate determining step, as we found that the adatom generation requires a larger barrier (1.1 to 1.3 eV) from a step edge surface (Supplementary Fig. 3). Additionally, our analysis revealed that the influence of CO* molecules in diminishing the barrier for Fe adatom generation is insignificant. Impurities such as CO and H known from an atomistic point of view, to promote surface reconstruction of Fe atoms[18]. Further research is necessary to investigate if the barrier for adatom generation can be lowered below the carbonyl formation barrier. Laycock et al.[19] have carried out an experimental study on
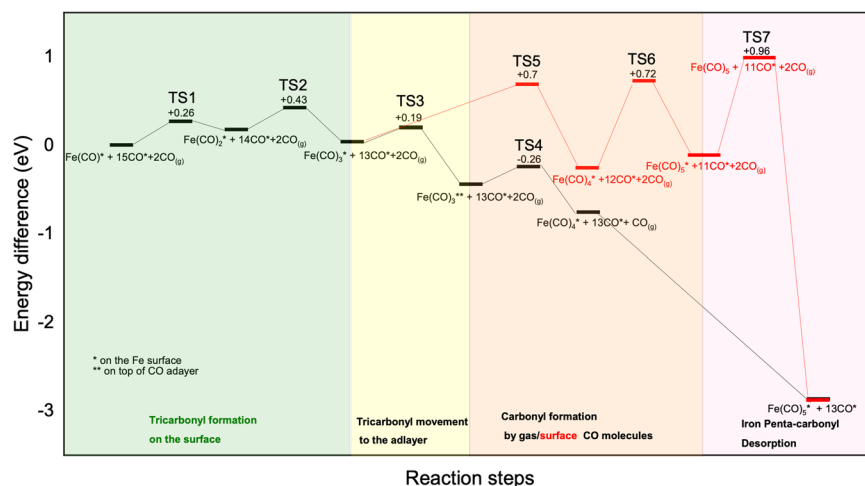
Fig. 6 Schematic representation of the proposed energetics of carbonyl formation on Fe(110) surface covered with 2/3 ML CO concentration on the surface. Colored areas represent the different phases the carbonyl goes during the reaction. The red reaction steps represent the case of the carbonyl totally forming on the surface, while the black colored path involves the Fe(CO)3 motion to adsorb on top of the CO molecules adlayer. TSx refers to the sequential series of transition state.

measurement of iron pentacarbonyl formation rates over low alloy steel surfaces under different conditions, as well as a result of different gaseous impurities in syngas. Under some of the conditions of experimental study, the steel surface was preconditioned via hydrogen stripping - allowing the bare alloy surface to subsequently react with syngas environment. The reaction energy surface that we propose in this present manuscript, allows one to potentially compare the resulting kinetics with the experimental data. We are currently actively working on this as a follow-up study and we expect in future to report it in subsequent papers/publications.

Finally, it is worth mentioning that the pretreatment of the surface and the presence of impurities such as S, H_2O and CO_2 can affect the carbonyl rate, as was experimentally proven[2]. Our future work will deal with the effect of these impurities on determining the rate determining step of carbonyl corrosion and how to mitigate it.

In conclusion, carbonyl corrosion is a potential problem for industry operating facilities with high pressure of carbon monoxide containing gases in the temperature range 400 K – 550 K. As CO is a significant component of many industrial processes from semiconductor fabrication to Gas to Liquid plants to fertilizer producers and any other industry using a steam methane reformer to generate synthesis gas. Although the reaction has been known for decades, no atomistic/molecular level model that explains the detailed reaction mechanism exists to the best of our knowledge. In this work, we put forward a scheme based on a large number of DFT calculations applied to different possible paths that lead to iron pentacarbonyl formation on iron surface in order to find the most probable reaction path. We found that the formation of carbonyls via purely surface diffusion and sequential insertion of CO^* molecules towards Fe adatom is unlikely on a pristine Fe(110) surface at low coverage of CO^*. High CO surface coverage is essential for carbonyl formation. Despite supporting carbonyls stability on the surface, CO^* molecule's vibration promotes the $Fe(CO)_3$ movement to the surface adlayer, leading to the detachment of iron tricarbonyl from the Fe surface atoms to stabilize on top of CO* molecules. This process requires an energy barrier of only 0.19 eV and a reverse barrier of 0.63 eV, making it very probable. The adsorption position of $Fe(CO)_3^{**}$ allows carbonyl to interact with gas molecules, leading to the formation of IPC with a barrierless desorption to the vacuum. We acknowledge, that the formation of Fe adatom itself on a clean or CO covered surface requires higher

barrier depending on the cleaved surface type for example. This work will set the foundation for future quest for the factors accelerating/slowing carbonyl corrosion and ways to mitigate it.

METHODS

Density functional theory calculations

We employed DFT to carry out energy minimization calculations and ab initio molecular dynamics simulations (AIMD). The projector augmented wave (PAW) pseudopotentials[20] with GGA-PBE exchange-correlation functional[21] was employed, as implemented within the Vienna ab initio Simulation Package (VASP)[22]. This includes benchmarking the influence of the number of monolayers within the considered slabs on the magnetic moment of the system, the van der Waals dispersion schemes as well as the planewave cutoff. Additionally, different minimization algorithms were tested, and found that the damped algorithm with *TIME* parameters as small as 0.02 leads to a slow but steady and consistent convergence of the SCF cycles[23]. Because of the large systems considered with volume > 4000 Å³, the Brillouin zone sampling was restricted to the Γ-point. Force symmetry breaking and a cutoff energy of 400 eV is used in all runs. DFT-D3 method with Becke Johnson damping function has been chosen in this work for describing accurate Van der Walls interactions[24].

Atomistic model construction

The reference model in this work consisted of an Fe(110) surface. It contains 120 Fe atoms across 5 atomic layers in a 3×4 supercell [see Fig. 7e] of dimensions 11.2 Å x 11.9 Å slab and a 20 Å vacuum along the z-direction. This Fe(110) surface supercell can accommodate up to 24 CO molecules to form one monolayer (1 ML), and is large enough to allow us to study the effect of CO concentrations while minimizing finite size effects. Ionic relaxation steps were performed using a convergence criteria of 10^{-4} eV for the total energy, equivalent to ~5 ×10^{-7} eV per atom. An Fe(211) model of 146 atom and 11.2 Å x 12.5 Å x 30.0 Å have been used for adatom generation calculation [see Fig. 7f].

On the Fe(110) clean surface with *n* adsorbed CO molecules ($n > 0$), out of which x CO molecules react with an Fe adatom to form the $Fe(CO)_x$ carbonyl species, then the carbonyl species'
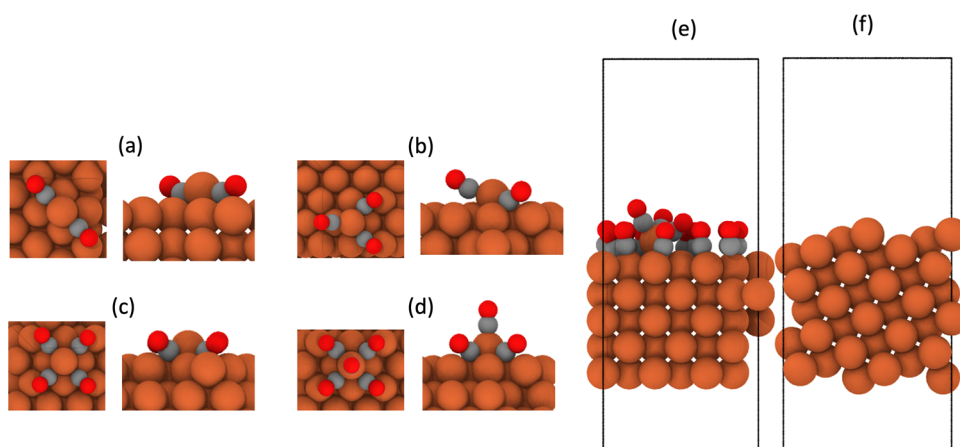
Fig. 7 Ball and stick representation of some the atomistic systems considered in this study. a–d Top and side views of the most stable adsorption position of carbonyls on clean Fe(110) surface, (**a**) represent $Fe(CO)_2^*$, (**b**) $Fe(CO)_3^*$, (**c**) $Fe(CO)_4^*$, and (**d**) $Fe(CO)_5^*$. **e** [100] view of Fe (110) slab model with an Fe adatom and ~0.6 ML CO coverage. **f** [100] view of Fe (210) slab model showing the step edge used in calculating the energetics of Fe adatom formation. Color code: oxygen in red, carbon in gray, and iron in brown.

adsorption energy can be defined as:

$$E_{Fe(CO)_x}^{ad} = E_{Fe(110)+(n-x)CO^*+Fe(CO)_x^*} - E_{Fe(110)+(n-x)CO^*} - E_{Fe(CO)_x(g)} \quad (1)$$

Where $E_{Fe(110)+(n-x)CO^*+Fe(CO)_x^*}$ is the energy of the system containing one $Fe(CO)_x^*$ and $(n-x)$ CO molecules adsorbed on Fe(110), $E_{Fe(110)+(n-x)CO^*}$ is the energy of the system without the carbonyl species on Fe(110) and $E_{Fe(CO)_x(g)}$ is the energy of the carbonyl species in the gas phase[25]. In the special case of $x = 0$, the left hand side term represents the adsorption energy of the Fe adatom.

The total binding energy (ΔE_B) of nCO adsorption on the Fe (100) surface is defined as:

$$\Delta E_B = E_{Fe(110)+nCO^*} - E_{Fe(110)} - E_{nCO}, \quad (2)$$

where ΔE_B is the total energy of Fe(110) surface with adsorbed CO molecules, $E_{Fe(110)}$ is the total energies of clean Fe(110) surface, n is the number of adsorbed CO molecules E_{nCO} is the total energy of n isolated CO*molecules in gas phase[14]. The average adsorption energy per molecule is the total binding energy divided by the number of CO molecules. The desorption energy is equal to or higher than the adsorption energy (in case of a presence of a barrier), hence estimating the adsorption energy should give us the lower bound for the desorption barrier.

Finally, the electronic charge-density difference is expressed as follows:

$$\Delta\rho(r) = \rho(r)_{Fe(110)+Fe(CO)_x^*} - (\rho(r)_{Fe(110)} + \rho(r)_{Fe(CO)_x^*}), \quad (3)$$

where $\rho(r)_{slab+carbonyl}$ is the electronic charge-density of the slab plus the adsorbed carbonyl species. $\rho(r)_{slab}$ and $\rho(r)_{carbonyl}$ are the electronic charge-density obtained from single point calculation of the slab and carbonyl coordinates system respectively[26].

Molecular dynamics and pathway construction

When placing molecular species manually on the surface adsorption sites and then geometrically relaxing the structure using DFT, biases may be introduced[27]. AIMD simulations aid to overcome such biases by providing information about the stability of the adsorbed molecular species at operating temperature (500 K) as well as to obtain an unbiased initial configuration. AIMD simulations were preformed within the canonical ensemble (NVT), where the number of atoms, volume, and temperature are kept constant, and using a time step of 1 fs. We used the Verlet algorithm combined to the Nosé–Hoover thermostat and heated the system from 50-500 K over 5000 fs.

For all elementary reactions of interest, we computed the transition state energies by using Nudged elastic band (NEB) calculations[28]. Our NEB calculations consist of 5 to 7 images run using the DFT setup detailed above and a total force convergence tolerance of 10^{-3} eV per Å. We generate the NEB pathways using the Halgren Lipscomb method as implemented in Quantum-Wise[27]. A careful relaxation of the initial and final points was conducted without fixing any atomic positions. This is done by using the AIMD calculations at 500 K to scan the configurational space of a stable configuration, by selecting the structure with the most stable energy in the selected timeframe and followed by DFT energy minimization.

DATA AVAILABILITY

The data needed to reproduce this work are available at the collaboration hub platform: https://aimater-collab.hbku.edu.qa/CollaborationHub/home?

CODE AVAILABILITY

No special codes/scripts were used in this work.

REFERENCES

1. Williams, T. C. & Shaddix, C. R. Contamination of carbon monoxide with metal carbonyls: implications for combustion research. *Combust. Sci. Technol.* **179**, 1225–1230 (2007).
2. Savitskaya, O. P. *Investigation of Carbonyl Corrosion in Metals* (Springer, 1968).
3. Lari, H. N. et al. Shedding light on iron pentacarbonyl photochemistry through a CVD case study. *Catal. Commun.* **100**, 19–23 (2017).
4. Mond, L. & Langer, C. XCIII.—On iron carbonyls journal of the chemical society. *Transactions* **59**, 1090–1093 (1891).
5. Cotton, F. A., Danti, A., Waugh, J. S. & Fessenden, R. W. Carbon-13 nuclear resonance spectrum and low-frequency infrared spectrum of iron pentacarbonyl. *J. Chem. Phys.* **29**, 1427–1428 (1958).
6. Inouye, H. & DeVan, J. H. Formation of iron carbonyl between a 1/2 pct Mo steel and high-pressure gases containing carbon monoxide. *J. Mater. Energy Syst.* **1**, 52–60 (1979).
7. Ricca, A. & Bauschlicher, C. W. J. Successive binding energies of Fe (CO) 5. *J. Phys. Chem.* **98**, 12899–12903 (1994).
8. Snee, P. T., Payne, C. K., Mebane, S. D., Kotz, K. T. & Harris, C. B. Dynamics of photosubstitution reactions of Fe (CO) 5: an ultrafast infrared study of high spin reactivity. *J. Am. Chem. Soc.* **123**, 6909–6915 (2001).

9. Brynestad, J. *Iron and Nickel Carbonyl Formation in Steel Pipes and Its Prevention-Literature Survey*. https://www.osti.gov/servlets/purl/7349456 (1976).

10. Cole-Filipiak, N. C., Troß, J., Schrader, P., McCaslin, L. M. & Ramasesha, K. Ultraviolet photodissociation of gas-phase iron pentacarbonyl probed with ultrafast infrared spectroscopy. *J. Chem. Phys.* **154**, 134308 (2021).

11. González-Blanco, O. & Branchadell, V. Density functional study of the Fe–CO bond dissociation energies of Fe(CO)5. *J. Chem. Phys.* **110**, 778–783 (1999).

12. Portius, P., Bühl, M., George, M. W., Grevels, F.-W. & Turner, J. J. Structure and dynamics of iron pentacarbonyl. *Organometallics* **38**, 4288–4297 (2019).

13. Cheng, H., Reiser, D. B., Dean, S. W. & Baumert, K. Structure and energetics of iron pentacarbonyl formation at an Fe(100) surface. *J. Phys. Chem. B* **105**, 12547–12552 (2001).

14. Yu, X. et al. CO adsorption, dissociation and coupling formation mechanisms on Fe2C (001) surface. *Appl Surf. Sci.* **434**, 464–472 (2018).

15. Wang, T. et al. Co-adsorption and mutual interaction of nCO+ mH2 on the Fe (1 1 0) and Fe (1 1 1) surfaces. *Catal. Today* **261**, 82–92 (2016).

16. Chakrabarty, A. et al. Elucidating the role of extended surface defects at Fe surfaces on CO adsorption and dissociation. *Appl. Surf. Sci.* **491**, 792–798 (2019).

17. Zaera, F. Mechanism for the decomposition of iron pentacarbonyl on Pt (111): evidence for iron tetracarbonyl and iron tricarbonyl intermediates. *Surf. Sci.* **255**, 280–288 (1991).

18. Li, X., Wang, Y., Huang, W., Zhang, J. & Wu, X. Effect of surface roughness on hydrogen-induced blister behavior in pure iron. *Met. (Basel)* **10**, 745 (2020).

19. Shivadhanush, B. R. et al. *Corrosion and Risk Modeling Analytics, AMPP Annual Conference and Expo*. https://ace.ampp.org/home (2023).

20. Blöchl, P. E. Projector augmented-wave method. *Phys. Rev. B* **50**, 17953 (1994).

21. Pedrew, J. P., Burke, K. & Ernzerhof, M. No Title. *Phys. Rev. Lett.* **77**, 3865 (1996).

22. Kresse, G. & Hafner, J. Norm-conserving and ultrasoft pseudopotentials for first-row and transition elements. *J. Phys. Condens. Matter* **6**, 8245 (1994).

23. Kresse, G. & Furthmüller, J. Efficient iterative schemes for ab initio total-energy calculations using a plane-wave basis set. *Phys. Rev. B* **54**, 11169 (1996).

24. Grimme, S., Ehrlich, S. & Goerigk, L. Effect of the damping function in dispersion corrected density functional theory. *J. Comput Chem.* **32**, 1456–1465 (2011).

25. Akande, S. O., Bentria, E. T., Bouhali, O. & El-Mellouhi, F. Searching for the rate determining step of the H2S reaction on Fe (110) surface. *Appl. Surf. Sci.* https://doi.org/10.1016/j.apsusc.2020.147470 (2020).

26. Akande, S. O. et al. Controlling surface chemistry of CO reactions on Fe surface by S blocking: a first-principles and microkinetic studies. *Appl. Surf. Sci.* https://doi.org/10.1016/j.apsusc.2021.151216 (2022).

27. Schneider, J. et al. ATK-ForceField: a new generation molecular dynamics software package. *Model Simul. Mat. Sci. Eng.* **25**, 85007 (2017).

28. Henkelman, G. & Jónsson, H. No Title. *J. Chem. Phys.* **113**, 9901 (2000).

AUTHOR CONTRIBUTIONS

Dr. Heesoo Park performed the DFT parameter benchmarking and optimization. Dr. El Tayeb Bentria carried out the DFT calculations and AIMD simulations on slab models, leading to reaction energy diagrams, and also wrote the first draft of the manuscript. Dr. Prathamesh Mahesh Shenai and Dr. Fadwa El-Mellouhi conceptualized the reaction mechanism and the computational methodology. Dr. Fadwa El-Mellouhi was also responsible for supervising researchers, the coordination of the team efforts and the fund acquisition. All authors conducted the literature review, fine-tuned the proposed methodology, analyzed the results and contributed in drafting and proof reading the manuscript.

COMPETING INTERESTS

The authors declare no competing interests.

ADDITIONAL INFORMATION

Supplementary information The online version contains supplementary material available at https://doi.org/10.1038/s41529-024-00429-x.

Correspondence and requests for materials should be addressed to Fedwa El Mellouhi.

Reprints and permission information is available at http://www.nature.com/reprints

Publisher's note Springer Nature remains neutral with regard to jurisdictional claims in published maps and institutional affiliations.